Novel six-axis robot kinematic model with axis-to-axis crosstalk

S. Ibaraki (2)[a,*], K. Fukuda[a], M. M. Alam[a], S. Morita[b], H. Usuki[b], N. Otsuki[c], H. Yoshioka[c]

a Graduate School of Advanced Science and Engineering, Hiroshima University, Kagamiyama 1-4-1, Higashi-Hiroshima 739-8527, Japan
b Institute of Industrial Science, The University of Tokyo, Chiba 277-8574, Japan
c Kawasaki Heavy Industries, Ltd., Gifu 504-8710, Japan

Conventionally, the volumetric error compensation of six-axis robots is mostly based on a kinematic model with position and orientation errors of the rotary axis average lines, known as Denavit–Hartenberg (D-H) parameters. This study proposes a novel kinematic model with angular positioning deviation of each rotary axis, modeled as a function of the command angle and rotation direction. The error motions of one rotary axis can be dependent on the angular position of other axes owing to changes in the moment of inertia or center of gravity. The prediction accuracy of the proposed model was experimentally evaluated. Compensation experiments showed a significant reduction in the static volumetric error over the entire workspace.
Robot; Accuracy; Positioning

1. Introduction

The application of industrial robots in machining has been actively studied [1]. A robot as a 'portable machine tool' can be a cost, space, and energy-efficient alternative to a large-sized machine tool [2]. An industrial robot is mostly programmed by the teach-in method, where a person operates the robot manually and is memorized by the robot. For machining operations, teach-in programming is no longer possible. When a robot is programmed based on a virtual model ("offline programming"), it critically requires sufficient volumetric accuracy over the entire workspace, similar to machine tools. The *volumetric error*, defined in [3], represents the 3D "absolute" positioning error from the command position over the entire workspace.

Numerous researchers have studied model-based compensation to improve a robot's volumetric accuracy. The Denavit-Hartenberg (D-H) model is the most primitive but most popular robot kinematics model [4]-[6]. The D-H model contains position and orientation errors of the rotary axis average lines as error sources. The *axis average line* [3] represents the mean position and orientation of the axis of rotation.

In many studies, even when the influence of the D-H parameters is compensated, a robot's volumetric error is still approximately 10 to 100 times larger than that of typical machine tools, for example, [7]. As the rotary axis rotates, its axis of rotation may be displaced or tilted as a function of its angular position. For machine tools, such angle-dependent errors are referred to as *error motions* [3]. The *angular positioning error motion* is a typical error motion of the rotary axis. In a robot, it is typically caused by tooth-to-tooth variations in the gear pitch error or the elastic deformation of the gear. Therefore, it is generally angle-dependent. The D-H parameters cannot describe such error motions because they are associated with the axis average line.

This study proposes a novel six-axis robot kinematic model containing the angular positioning deviation of each rotary axis, in addition to the D-H parameters. The angular positioning deviation is modeled as a function of its command angle, and additionally the rotation direction, to model the influence of backlash.

Moreover, the error motions of one rotary axis can be dependent on the angular position of the other axes, owing to the change in the moment of inertia or center of gravity. This paper presents the measurement, and modeling of the *axis-to-axis crosstalk*. In [8], the authors partly presented a robot model with rotary axis angular positioning deviations. The inclusion of the axis-to-axis crosstalk is an original contribution of this study.

In the robotics community, researchers have presented robot models with influencing factors other than the D-H parameters. The inclusion of the joint or link stiffness has been studied by many researchers [9]–[11]. The influence of the joint friction and backlash was modeled in [12]. Nubiola and Bonev [13] presented the measurement of the angular positioning error motion of rotary axes using a tracking interferometer; however, they did not present its integration into the kinematic model of the robot. None of the previous works presented the extension of the D-H model to the rotary axis error motions with the aim of modeling the volumetric error over the entire workspace.

However, model-based volumetric error compensation has been extensively studied in the machine tool community [14][15]. Essentially, this study can be regarded as an extension of the model-based indirect measurement of error motions in industrial robots; a crucial difference is in the kinematic model.

2. Proposed model
2.1. Conventional kinematic model

This study considers the six-axis robot configuration shown in Fig. 1. The objective of the kinematic model is to formulate the k-th end effector position in the reference coordinate system (CS), denoted by $^r\hat{p}(k) \in \Re^3$ (the left-hand side superscript represents the CS), when the command angular position of the A_n-axis ($n=1, ..., 6$) is given by $\theta_n^*(k) \in \Re$. It is given by:

$$\begin{bmatrix} ^r\hat{p}(k) \\ 1 \end{bmatrix} = \ ^rT_6 \cdot \begin{bmatrix} ^6p \\ 1 \end{bmatrix}. \tag{1}$$

$$^rT_6 = \ ^rT_1 \cdot \ ^1T_2 \cdot \ ^2T_3 \cdot \ ^3T_4 \cdot \ ^4T_5 \cdot \ ^5T_6 \tag{2}$$
$$^rT_1 = D_c(\theta_1^*(k))$$
$$^1T_2 = D_x(L_{1x} + \delta x_{21})D_z(L_{1z})D_a(\alpha_{21})D_b(\theta_2^*(k) + \Delta\theta_{20})$$
$$^2T_3 = D_z(L_{2z} + \delta x_{32})D_a(\alpha_{32})D_c(\gamma_{32})D_b(\theta_3^*(k) + \Delta\theta_{30})$$
$$^3T_4 = D_z(L_{3z} + \delta z_{43})D_y(\delta y_{43})D_c(\gamma_{43})D_a(\theta_4^*(k) + \Delta\theta_{40})$$
$$^4T_5 = D_x(L_{4x} + \delta x_{54})D_z(\delta z_{54})D_c(\gamma_{54})D_b(\theta_5^*(k) + \Delta\theta_{50})$$
$$^5T_6 = D_z(L_{5x})D_z(\delta z_{65})D_y(\delta y_{65})D_c(\gamma_{65})D_a(\theta_6^*(k))$$

$^6p \in \Re^3$ is the tool vector given in the A_6-axis CS. $D_*(\dagger) \in \Re^{4 \times 4}$ denotes the homogeneous transformation matrix (HTM) representing the linear translation to the X-, Y-, and Z-directions (for *: x, y, z) by the distance $\dagger \in \Re$, or the rotation around the X-, Y-, and Z-axes (for *:

a, b, c) by the angle †. Their formulation is given in [15] and is omitted in this paper. $L_* \in \Re$ represents the nominal link length. The other 18 parameters, for example, δx_{21}, α_{21}, $\Delta\theta_{20}$, ..., are the D-H parameters. See [8] for their definitions (omitted in this paper).

The kinematic model (1) has been presented in many previous publications and is not a part of this study's new contributions.

2.2. Proposed model with rotary axis angular positioning deviations

The first original contribution of this study is the inclusion of the angular positioning deviation of each rotary axis in the kinematic model (1) as error sources. For the prescribed set of A_n-axis command angular positions, $\theta_{n,map}{}^*(i_n) \in \Re$, where $i_n \in \Re$ is the index number (i_n=1, ..., N_n), the angular positioning deviation is represented by $\Delta\theta_{n,map}(i_n, \pm1)$, with +1 when the angular velocity is positive, and -1 when negative. In other words, the angular positioning deviation is modeled as a function of the command angular position and rotation direction to model the gear backlash.

When the A_n-axis command angle is arbitrarily given by $\theta_n{}^*(k)$, its actual angular position is estimated by linearly interpolating $\Delta\theta_{n,map}(i_n, \pm1)$. Then, the end effector position, ${}^r\hat{p}(k)$, can be estimated by replacing $\theta_n{}^*(k)$ in the model (2) with it. Higher-order interpolation, for example polynomial or B-spline fitting, is possible; however, it is not employed in this study because its influence is minor compared to the robot's positioning repeatability.

2.3. Measurement of angular positioning deviations

Fig. 1 illustrates the proposed measurement setup. The test objective was to identify the angular positioning deviation of the A_n-axis, $\Delta\theta_{n,map}(i_n, \pm1)$ for all i_n=1, ..., N_n in both directions (+1 and -1), as well as all the D-H parameters included in Eq. (2).

A cat's eye retroreflector was mounted on the robot end effector. The A_n-axis was indexed at every command angle $\theta_{n,map}{}^*(i_n)$. All other axes were fixed at the prescribed reference angular position. The retroreflector's 3D position was measured using a tracking interferometer (laser tracker) at each stop position. This test is performed bidirectionally, and is performed for every rotary axis.

The center of the best-fit circle to the measured trajectory and its orientation define the axis average line, thus give the D-H parameters. The angular positioning deviation can then be identified from the measured trajectory on the local CS, defined based on the axis average line. A detailed algorithm is presented in [8].

2.4. Axis-to-axis crosstalk

The measurement and modeling of the axis-to-axis crosstalk is another new contribution of this study. Figure 2 shows an illustrative example. When the A_3-axis is indexed at different angles, the moment of inertia with the A_2-axis rotation changes. It can change its motor load, and subsequently, the A_2-axis angular positioning deviation. This influence can be included in the proposed model by making the angular positioning deviation dependent on the angular position of the other axis. In this example, the A_2-axis angular positioning deviation is modeled by $\Delta\theta_{2,map}(i_2, \pm1, i_3)$, where i_3 represents the index number of the A_3-axis angular position.

Analogous axis-to-axis crosstalk can also be observed on machine tools [16][17]; however, its influence can be significantly larger on a robot.

By integrating the axis-to-axis crosstalk into the model, Fig. 3 outlines the input/output relationship of the proposed model.

3. Experiment

3.1. Identification of angular positioning deviations

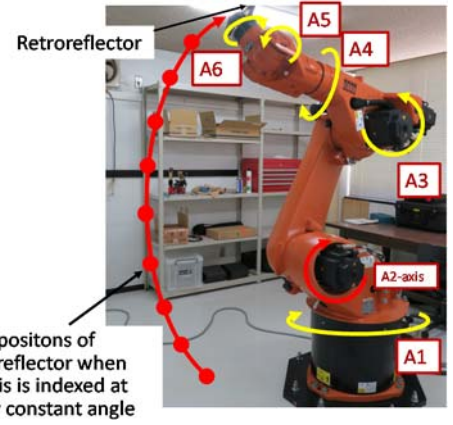A six-axis robot, KUKA KR30HA, shown in Figs. 1 and 2, was

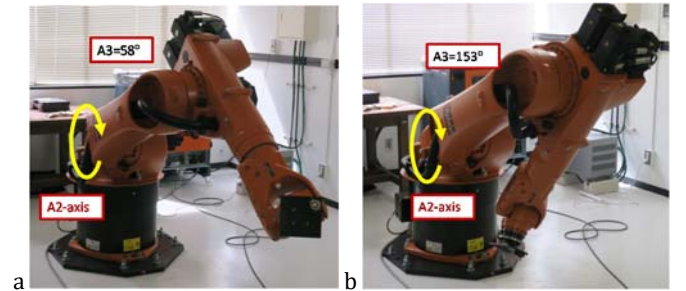**Figure 1.** Robot configuration and measurement scheme of the rotary axis angular positioning deviation of A_2-axis.

Figure 2. First example of axis-to-axis crosstalk: A_2-axis angular positioning deviation is measured with a) A_3-angle $\theta_3{}^*$=58°, and b) $\theta_3{}^*$=153°.
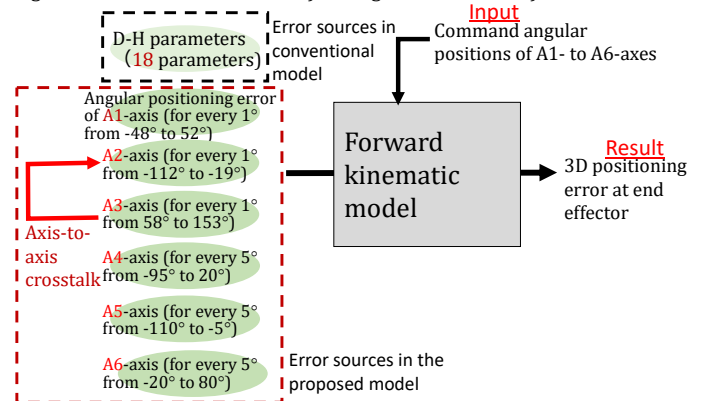

Figure 3. Input/output relationship of the proposed model (the command angles are for the setup in Section 3)

measured (maximum reach: 2033 mm; rated payload: 30 kg). A tracking interferometer (Leica AT960-XR) was used. First, the bidirectional angular positioning deviations of the A_1- to A_6-axes were identified by applying the test proposed in Section 2.3. For example, the A_2-axis indexing test measured a total of 186 points (from -112° to -19° at every 1°, bidirectionally) and took approximately 10 minutes. As an example, Fig. 4 shows the identified bidirectional angular positioning deviation profiles of the a) A_1- and b) A_2-axes. They exhibit a periodic variation with the period attributable to the gear pitch.

3.2. Axis-to-axis crosstalk

Figure 5 shows a comparison of the identified A_2-axis angular positioning deviations with three different A_3-axis angular positions (see Fig. 2). The crosstalk influence is evident.

Second significant axis-to-axis crosstalk was observed in this robot: the influence of the A_2-axis angle on the A_3-axis angular positioning deviation. As shown in Fig. 6, the A_3-axis angular positioning deviation was measured with the a) A_2-axis angle $\theta_2{}^*$=-112°,

and b) θ_2^*=-19. Figure 7 shows the A_3-axis angular position deviation measured under three different A_2-axis angles. It is predictable that the deviation in the A_3-axis angular position is influenced by the gravity imposed on its arm (from the third link to the end effector). The A_2-axis angle changes the direction of the arm to gravity. This is most likely the major cause of this crosstalk.

3.3. Prediction performance of the proposed model

The accuracy of the proposed model was evaluated using three rectangular paths, as shown in Fig. 8. The three paths are over X400×Y2,000×Z1,000 mm and cover a large portion of the robot's workspace. When the robot was positioned at each stop position (in 100 mm pitch) on the paths, its 3D position was statically measured by the tracking interferometer, and then compared to the predicted trajectory. The influence of the A_3-axis angle on the A_2-axis angular positioning deviation, shown in Fig. 5, was included in the prediction model. The crosstalk shown in Fig. 7 was not included because its influence on the end effector positions was smaller, according to numerical simulation with the proposed model.

For Path 1, Fig. 9 compares a) the measured trajectories on the XY plane, b) the simulated trajectories by the proposed model, and c) the simulated trajectories by the conventional model with the D-H parameters only. The errors from the command positions are magnified 1,000 times (see "Error scale"). Compared to Fig. 9c, Fig. 9b shows a significantly better prediction performance. Fig. 9d shows the difference between (a) and (b).

For Path 1, Fig. 10 compares a) the measured errors in the Z-direction and b) the simulated errors by the proposed model without including the crosstalk of A_3 angle on the A_2 angular positioning deviation, and c) the simulated one with the crosstalk. The prediction performance in Fig. 10c is improved compared to Fig. 10b.

3.4. Compensation

When the end-effector position is estimated by the proposed model (1), the command position, $^rp^*(k)$, is modified to

$$^rp_{\text{comp}}^*(k) = {}^rp^*(k) - ({}^r\hat{p}(k) - {}^rp^*(k)), \tag{3}$$

This compensation was applied to Paths 1 to 3. Fig. 9e shows the compensated trajectories in the XY plane. Figure 11 shows histograms of the distribution of the error in the XY plane (in column "a") and in the Z-direction (in column "b"). Table 1 summarizes the mean and two σ (σ standard deviation) of the histograms in Fig. 11. By the compensation based on the proposed model with the axis-to-axis crosstalk, the positioning error was reduced from 1/2 to 1/3 in both the mean and two σ over the three paths.

4. Conclusion

- An essential limitation of the conventional D-H model is that it only contains the position and orientation errors of the rotary axis average lines as error sources. This study presented an extended model with angle- and direction-dependent angular positioning error motions of all the axes. Furthermore, a scheme to measure the axis-to-axis crosstalk on the angular positioning deviations and its inclusion in the model are presented.
- On the rectangular paths, the proposed model showed significantly better prediction accuracy than the conventional D-H model. Furthermore, by including the crosstalk influence of the A3-axis angle on the A2-axis angular positioning deviation,

The velocity and acceleration can influence the static positioning error, possibly owing to the elastic deformation of the gears. The inclusion of such an influence may further improve compensation performance. Furthermore, the tool orientation error can also deteriorate the machining accuracy. The proposed model can potentially be extended to tool orientation. Robots of different serial-link kinematic configurations can be analogously modeled, and the extension of the method to parallel-link kinematics is also possible.
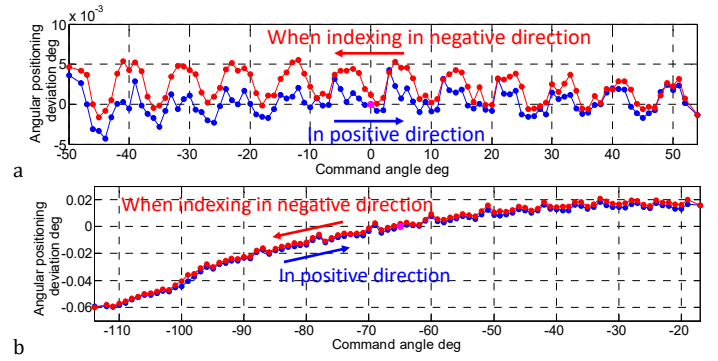

Figure 4. Bidirectional angular positioning deviation profiles identified by the proposed scheme. a) A_1-axis, b) A_2-axis.
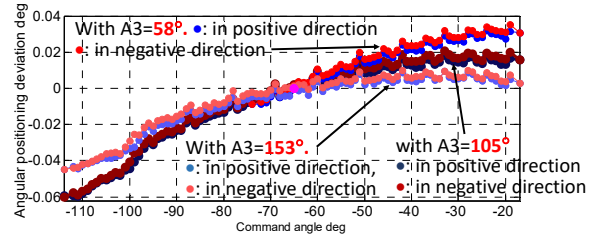

Figure 5. Measured Influence of A_3-angle (θ_3^*=58, 105, and 153°) on A_2-axis angular positioning deviation (in positive and negative directions)
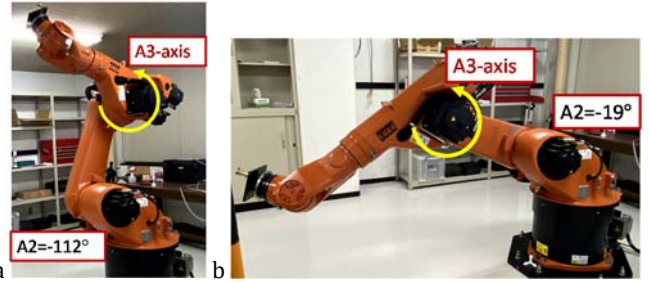

Figure 6. Second example of axis-to-axis crosstalk: A_3-axis angular positioning deviation is measured with a) A_2-angle, θ_2^*=-112°, and b) θ_2^*=-19°
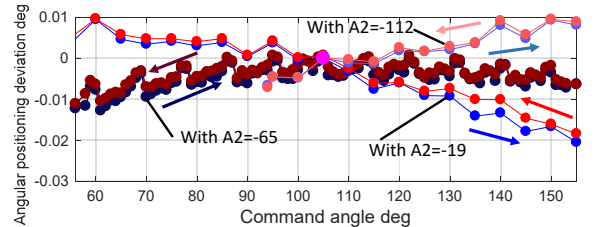

Figure 7. Measured Influence of A_2-angle (θ_2^*=-19, -65 and -112°) on A_3-axis angular positioning deviation (in positive and negative directions)
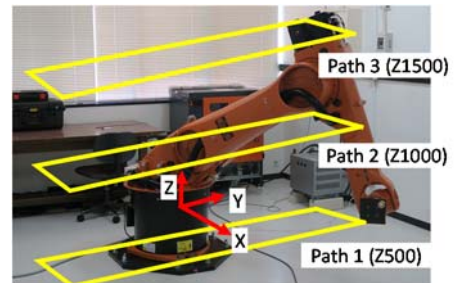

Figure 8. Three paths for model validation (X400 × Y2000 mm)

In the case of the latter, the model identification may not be straightforward because the individual axes cannot be driven independently.
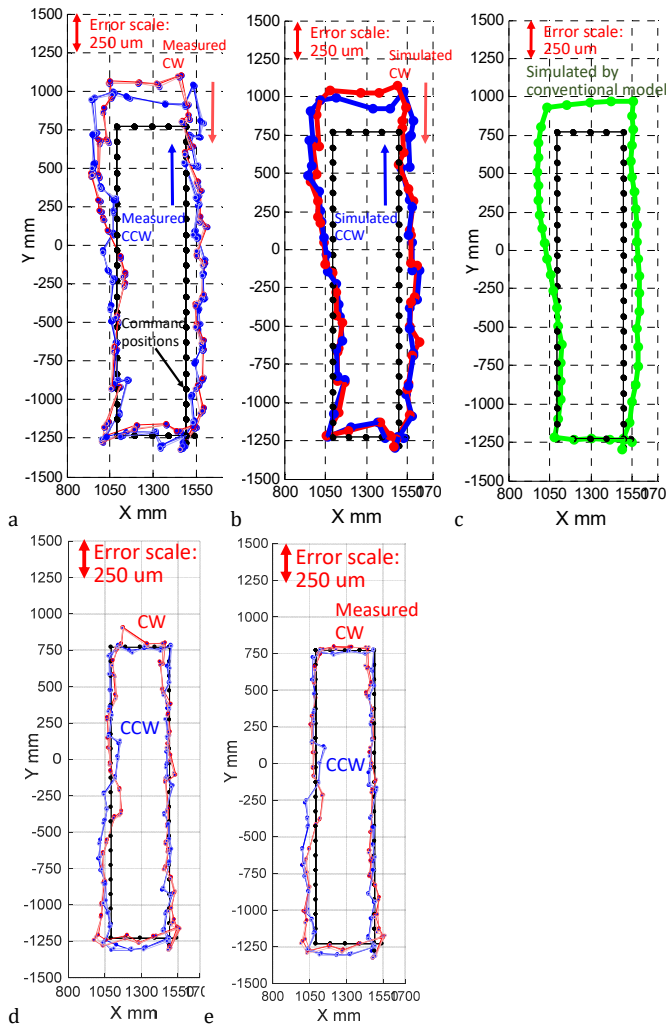
Figure 9. Comparison of positioning errors on the XY plane in Path 1 (at Z500 mm) a) measured by tracking interferometer (measured three times), b) simulated by the proposed model, c) simulated by the conventional model with 18 D-H parameters only; d) difference between a) and b), and e) measured under the compensation by the proposed model.
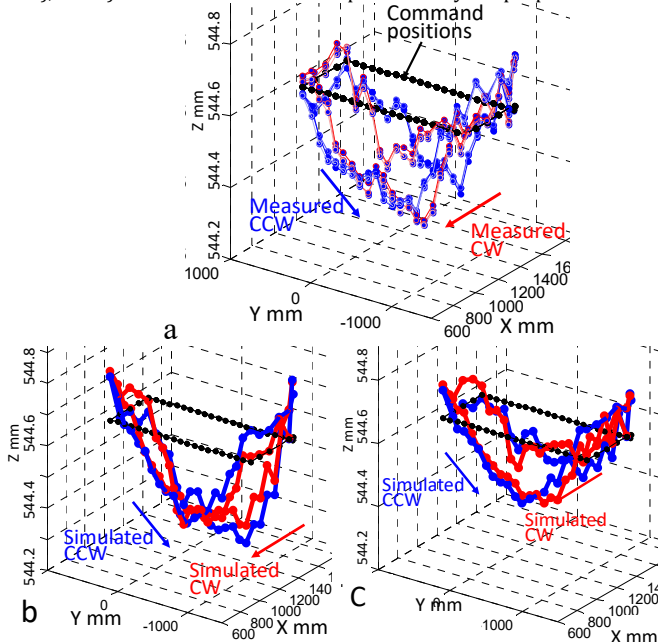

Figure 10. Comparison of positioning errors in Z direction on Path 1, a) measured by tracking interferometer (measured three times), b) simulated by the model without the axis-to-axis crosstalk, and c) simulated by the full model with the axis-to-axis crosstalk.
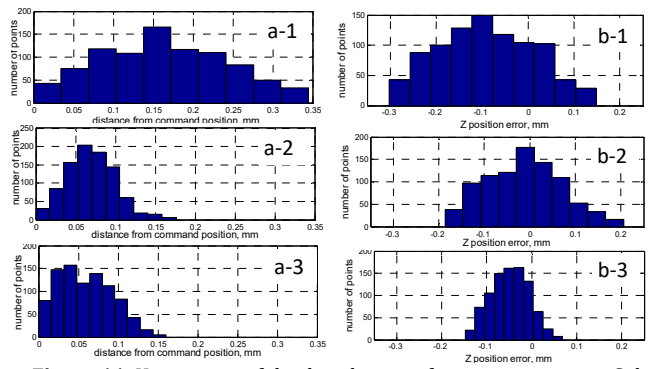

Figure 11. Histograms of the distribution of positioning errors. Column "a": error (distance) in the XY plane, "b": error in the Z-direction. Row "a/b-1": the distribution of uncompensated trajectories, "a/b-2": the compensated trajectories by the model without the axis-to-axis crosstalk, and "a/b-3": the compensated trajectories by the full model.

Table 1. Summary of the histograms in Fig. 11

	Error in XY		Error in Z	
	Mean	2σ	Mean	2σ
Uncompensated	163 μm	158 μm	-90 μm	206 μm
Compensated (proposed model without axis-to-axis crosstalk)	70 μm	60 μm	-12 μm	164 μm
Compensated (with axis-to-axis crosstalk)	59 μm	66 μm	-48 μm	82 μm

References

[1] Verl A, Valente A, Melkote S, Brecher C, Ozturk E, Tunc LT (2019) Robots in machining, CIRP Annals -- Manufacturing Technology, 68(2): 799–822.

[2] Uriarte L, Zatarain M, Axinte D, Yagüe-Fabra J, Ihlenfeldt S. Eguia J, Olarra A (2013) Machine tools for large parts, CIRP Annals--Manufacturing Technology, 62(2): 731-750.

[3] ISO 230-1:2012, Test code for machine tools -- Part 1: Geometric accuracy of machines operating under no-load or quasi-static conditions.

[4] Watanabe A, Sakakibara S, Ban K, Yamada M, Shen G (2006) A Kinematic Calibration Method for Industrial Robots Using Autonomous Visual Measurement, Annals of CIRP, 55(1): 1-6.

[5] Alici G, Shirinzadeh B (2005) A systematic technique to estimate positioning errors for robot accuracy improvement using laser interferometry based sensing, Mechanism and Machine Theory, 40(8): 879-906.

[6] Filion A, Joubair A, Tahan AS, Boneva IA (2018) Robot calibration using a portable photogrammetry system, Robotics and Computer-Integrated Manufacturing, 49: 77-87.

[7] Wu Y, Klimchik A, Caro S, Furet B, Pashkevich A (2015) Geometric calibration of industrial robots using enhanced partial pose measurements and design of experiments, Robotics and Computer-Integrated Manufacturing, 35: 151-168.

[8] Fukuda K, Ibaraki S. Alam MM, Morita S, Usuki H, Otsuki N, Yoshioka H (2020) Identification of a novel kinematic model of a 6-DOF robot with bidirectional angular positioning deviation of rotary axes, Proc. of 18th International Conference on Precision Engineering.

[9] Abele E, Weigold M, Rothenbücher S (2007) Modeling and identification of an industrial robot for machining applications, CIRP Annals--Manufacturing Technology, 56(1): 387–390.

[10] Theissen NA, Laspas T, Archenti A (2019) Closed-force-loop elastostatic calibration of serial articulated robots, Robotics and Computer Integrated Manufacturing, 57: 86–91.

[11] Kamali K, Bonev IA (2019) Optimal Experiment Design for Elasto-Geometrical Calibration of Industrial Robots, IEEE/ASME Transactions on Mechatronics, 24(6): 2733-2744.

[12] Slamani M, Nubiola A, Ilian IA. Bonev (2012) Modeling and assessment of the backlash error of an industrial robot, Robotica, 30(7):1167-1175.

[13] Nubiola A, Bonev IA (2014) Absolute robot calibration with a single telescoping ballbar, Precision Engineering, 38(3): 472–480.

[14] Schwenke H, Knapp W, Haitjema H, Weckenmann A, Schmitt R, Delbressine F (2008) Geometric Error Measurement and Compensation of Machines – An Update, CIRP Annals -- Manufacturing Technology, 57(2): 560-575.

[15] Ibaraki S, Knapp W (2012) Indirect Measurement of Volumetric Accuracy for Three-Axis and Five-Axis Machine Tools: A Review, Int. J. Automation Technology, 6 (2): 110-124.

[16] Ibaraki S, Hiruya M (2020) Assessment of non-rigid body, direction- and velocity-dependent error motions and their cross-talk by two-dimensional digital scale measurements at multiple positions, Precision Engineering, 66: 144-153.

[17] Bringmann B, Maglie P (2009) A method for Direct Evaluation of the Dynamic 3D Path Accuracy of NC Machine Tools, CIRP Annals - Manufacturing Technology, 58(1): 343-346.